SSC24-S3-08

Automated design and validation of acquisition patterns for optical inter-CubeSat links

René Rüddenklau, Jorge Rosano Nonay
Institute of Communications and Navigation, German Aerospace Center (DLR)
Münchener Straße 20, Weßling, 82234, Germany
rene.rueddenklau@dlr.de

Georg Schitter
Automation and Control Institute (ACIN), TU Wien
Gußhausstrasse 27-29, Vienna, 1040, Austria

ABSTRACT

Commercially available CubeSats with volumes of up to six units cannot achieve the precision required for an instantaneous establishment of a low-divergence optical inter-satellite link employing solely their attitude-determination and control system. Those residual attitude errors are present due to vibrations and limited control precision caused by the commonly used reaction wheel actuators. Thus, search patterns are used to scan the remaining field of uncertainty in order to achieve an optical inter-satellite. This work focuses on the development of an automated procedure to optimize the interaction between each of the individual search patterns. The performance of the two combined patterns is measured by their mean acquisition time and probability of success based on a Monte-Carlo simulation. Four patterns – Spiral, Rose, Lissajous and Grid – are considered and modified according to the optical inter-satellite link scenario between two CubeISL laser communication terminals. They are distinguished by their respective tasks within the acquisition scheme. The terminal for pointing, acquisition and tracking (T-PAT) scans the field of uncertainty in order to establish the link. The terminal for detection, adjustment and tracking (T-DAT) scans for a hit on its optical detector with a matched pattern period. It then gradually compensates for the remaining error until both terminals can switch to active tracking mode.

The proposed acquisition scheme and generated patterns were verified in a campaign over 334 m link distance. To achieve a controllable test environment, both CubeISL terminals and attitude manipulation actuators were automated. This approach offers the advantage of repeatable parameter variations and a higher number of tests that can be carried out. Each run takes approximately 10 minutes, which emulates the envisaged runtime in space, including the configuration of the terminals and supporting equipment. Additionally, all configurations are executed multiple times to evaluate the standard deviation of individual tests. The presented procedure demonstrates that simulations can exclude a significant number of design parameter combinations. The remaining pattern sets are implemented for final optimization during a field-test with the actual hardware of the optical terminals. As both CubeSats will operate in space without real-time supervision, the same validation process can be applied during commissioning. Therefore, the proposed automated design and validation procedure reduces the time required for supervised measurement campaigns while increasing confidence in the reliability of the overall system for remote on-orbit operation.

INTRODUCTION

Optical free-space communication is characterized by high transmission rates. However, this also means that the divergence of the beam should be very low in order to make the best use of the available emitted optical power on a CubeSat. This leads to increased pointing accuracy requirements for the entire spacecraft attitude control system, including the fine pointing assembly of the optical terminal. In particular, during the acquisition phase, when optical feedback is temporarily unavailable, precise attitude knowledge is essential. Since no high-speed data exchange can take place during the initial acquisition phase, it is an important requirement of the laser communication terminal (LCT) to reduce the time for establishing a link. Approaches to optimize this task already exist. It has been investigated which type of search pattern can be used most effectively[1]. Analytical approaches have also been proposed and metrics such as mean acquisition time and success probability have been introduced[2,3]. Furthermore, it has been investigated to what extent external disturbances affect the process, which requires a statistical evaluation[4–6]. On closer examination, none of the mentioned works investigates the case of two 6U CubeSats. Further, this work includes implicit bandwidth constraints imposed by the

mechatronic devices used, such as a fine steering mirror (FSM) and attitude control systems, in combination with a pattern-based optimization approach.

The main contribution of this work is the analysis of acquisition patterns for an optical inter-satellite link (OISL) by optimizing the probability of success and the expected acquisition time duration, considering the dynamics of the involved system components. The best performing combination of acquisition patterns with respect to these metrics have been identified. The design of an acquisition scheme including the baseline pattern Spiral and Grid has already been considered in a preliminary analysis[7]. However, this work did not include detailed consideration of the perturbations, but was oriented towards a feasible concept. The following work will focus on the first acquisition hit. This is the most critical event in the acquisition phase, as it contains information about the attitude with respect to the counterpart terminal. Consider that, due to the acquisition scheme (see Figure 1), additional time is required after the first hit occurred to achieve a bidirectional link. The optimization algorithm proposed in this work will select a pair of search patterns based on the given system design and its application environment, and optimize them accordingly. It is capable of predicting the performance including the assembled actuator and sensor and therefore improves the estimation results of the expected performance compared to existing work.

CUBEISL SYSTEM ANALYSIS

CubeISL is a project by the German Aerospace Center (DLR) and its Institute of Communications and Navigation. The Optical Satellite Links Department, who has also developed the predecessor OSIRIS4CubeSat for the PIXL-1 mission[8], is in charge of designing, testing and verifying this 1U payload. In Figure 1 the acquisition scheme as developed for CubeISL is presented. The simulation part of this analysis focuses on phase (a), the initial search, where no hits have yet been detected. Sketched are the slow scanning Grid pattern in combination with a Spiral.

The subsequent phases deal with the challenge that both LCTs have to precisely align themselves to each other after the acquisition hit occurred and decide when a tracking lock has been achieved, which will be investigated in the experimental part of this work. The CubeISL pair of terminals A and B are only distinguished by their respective transmit and receiving wavelengths. They are interchangeable in software, allowing both to operate as T-PAT (terminal for pointing, acquisition and tracking) or T-DAT (terminal for detection, adjustment and tracking), which determines their behavior during acquisition.

As the actual switching to tracking mode presents its own challenges, it should be noted that improvements to the bidirectional closed-loop control is part of an ongoing work. Nevertheless, first tests are carried out with the experimental setup presented below. The defined set of system parameters determines the specific challenges of the envisaged optical ISL. The scenario in this work is closely related to the CubeISL project but is of general interest for similar projects. This 1U optical payload inside a 6U CubeSat, shown in Figure 2, is designed to establish an ISL of up to 1500 km between two low earth orbit satellites[9].

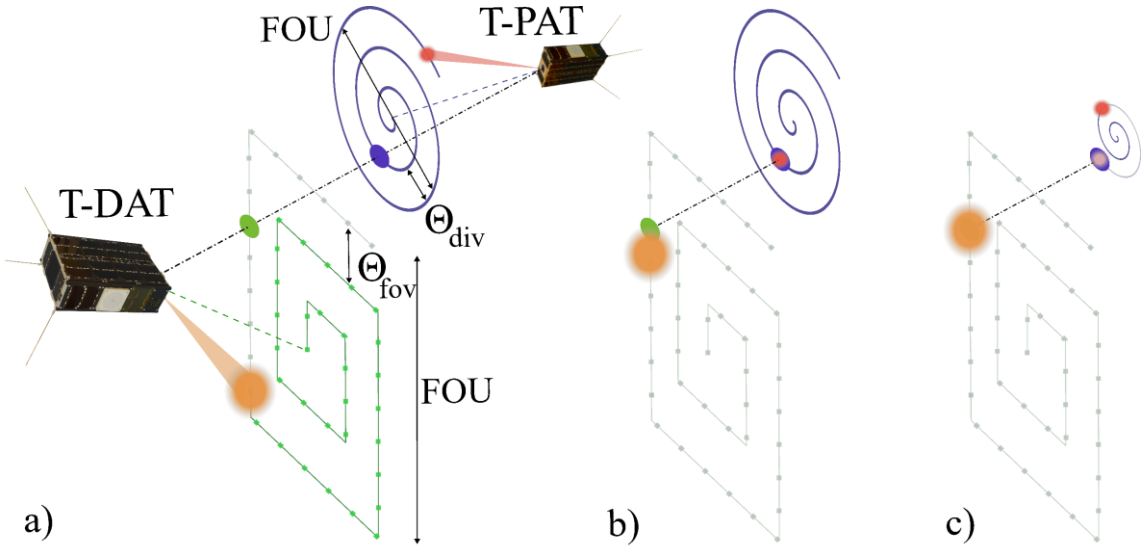

Figure 1: Brief sequence of the acquisition scheme. With (a) searching for an initial hit. (b) Step-wise adjustments of Terminal(T-DAT) by reoccurring hits from Terminal(T-PAT). (c) Terminal(T-DAT) is aligned within the accuracy of its divergence angle Θ_{div}, waiting for Terminal(T-PAT) to acquire (indicated with grey spiral).

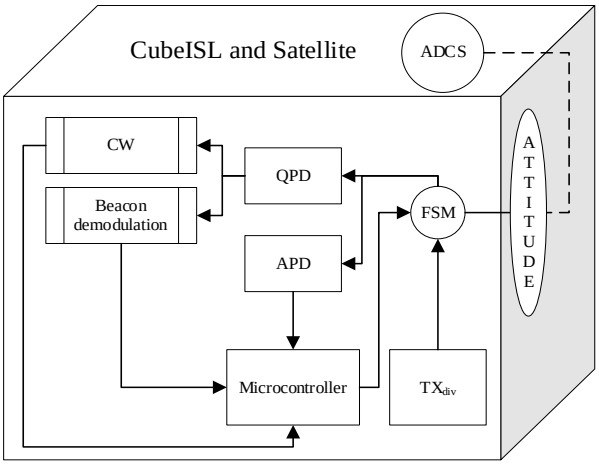

Figure 2: Schematic of the interdependencies between components within the CubeISL system and the 6U CubeSat's attitude determination and control system (ADCS).

The ADCS system of the satellite is coupled to the optical system via the aperture of the system due to the attitude with respect to the link partner. In CubeISL, the transmit (TX) path is overlapping with the receive (RX) path and both are therefore simultaneously manipulated via the FSM. The quadrant photo diode (QPD) features two independent evaluation electronics which can detect either continuous wave (CW) or modulated beacon signals.

A condensed set of system parameters with high impact on the scenario are summarized in Table 1. All standard deviations are given as 3σ. The field of uncertainty (FOU) is considered to be the radial magnitude of the maximum uncertainty from the actual target. This range is limited to ±1 degree due to the design of the optical system. For the ISL case, only a subset of FOU has been considered, as shown later in Figure 4 and Figure 5, where exponentially increasing search times are expected to exceed the time limit t_{lim} and thus the power budget of the mission. Therefore, if a link in CubeISL is not established within 10 minutes, the acquisition is cancelled and the satellite is reorientated to recharge the batteries. A new attempt can be made thereafter.

The full divergence angle Θ_{div} at $1/e^2$ and the field of view (FOV) $\Theta_{QPD/APD}$ are design parameters of CubeISL and play a decisive role in the results of the analysis. Since the simulation shall lead to a direct result for experimental tests, it is important to use the parameters from the LCT. In Table 1 are two bandwidths mentioned for the QPD. This is due to the fact that the electronics are able to perform beaconless acquisition with the data signal, which is received as CW by the QPD, or with a dedicated beacon using a 10 kHz modulation (see Figure 2). The latter is particularly useful in scenarios with significant background light and power fades due to atmospheric effects in direct-to-earth links. The demodulation electronics provide a bandwidth of 200 Hz for the modulated channel and 1.59 kHz for the CW channel.

Table 1: Scenario parameters of the OISL using two CubeISL CubeSat LCTs.

Symbol	Value	Unit
Θ_{div}	$192.8 \cdot 10^{-6}$	rad
$\Theta_{QPD,MOD}$	$1.326 \cdot 10^{-3}$	rad
$BW_{QPD,MOD}$	200	Hz
$BW_{QPD,CW}$	$1.59 \cdot 10^{3}$	Hz
Θ_{APD}	$1.935 \cdot 10^{-3}$	rad
BW_{APD}	$3.5 \cdot 10^{3}$	Hz
BW_{FSM}	72	Hz
f_R	280	Hz
$3\sigma_{FOU}$	$[0.1, 0.2, 0.3, 0.4, 0.5]$	deg
$3\sigma_{vib}$	$10 \cdot 10^{-6}$	rad
$3\sigma_{drift}$	0.08	deg/s
t_{lim}	$[60, 600]$	s
t_a	0.002	s
p	1600	-
t_s	0.001	s

Furthermore, the ability of the data receiver to support the acquisition is investigated in the simulation. The advantages of using an avalanche photo diode (APD) as the acquisition sensor are the increased FOV obtained in this design and the higher bandwidth based on an estimate from preliminary tests. The disadvantage of using the data sensor for acquisition is due to the APD itself which cannot provide information about the location of a hit. However, the deflection of the FSM can be used as a reference to determine the angular offset in the event of a valid signal. The introduced $3\sigma_{vib}$ are a combination of attitude control jitter and micro-vibrations. The $3\sigma_{drift}$ results from the limited precision of the satellite's control system, which causes it to tumble around the target position. The motion is not necessarily Gaussian distributed as it depends on the active closed loop control of the ADCS.

OPTICAL INTER-SATELLITE LINK PATTERN OPTIMIZATION

A Monte Carlo simulation has been chosen as the analysis tool because this work involves randomly distributed disturbances that could only be tested at great expense on a hardware breadboard. In addition, this simulation will be nested within a tool that takes characteristic link parameters as input and optimizes selected pattern combinations in terms of their probability of success (SR) and mean acquisition time (MAT).

Dual-Scan pattern optimization

The implemented optimization framework (see Figure 3) considers predefined hardware design parameters of the LCT, such as

- actuation sampling time (fixed pattern) t_a,
- pattern resolution p,
- actuator bandwidth BW_a,
- controller signal sampling time t_s,
- design and environment $\Theta_{div}, \Theta_{fov}, \sigma_{FOU}, \sigma_{vib}, \sigma_{drift}$,
- sensor bandwidth BW_s,

and variables that can be adapted to reach the desired performance

- actuation sampling time (optimization pattern) α,
- pattern resolution and amplitude factor β, δ,
- optimization weighting factors $\gamma_{1\dots4}$ and $\gamma_{\alpha_1}, \gamma_{\alpha_2}$.

The optimization in Figure 3 starts by generating the trajectory Tr, which is is bounded by the resolution p, that also defines the time period $T_{pattern} = t_a \cdot p$ for one full scan. The pattern is scaled in amplitude and resolution using the variables β and δ. In the second step, dynamics are introduced by using the transfer function of the used actuator A. Its bandwidth BW_a and the current actuation time α determine the actual trajectory of the pattern. In the third step, the processing capabilities of the processor unit are considered. In this example, $t_s = 0.001$ s is used and therefore determines the sampling interval between two evaluation steps at which a hit can be identified by the system. As a last step in the pattern optimization routine, the two optimization parameters δ and β are used to adapt amplitude and resolution of the pattern, considering the influence of the simulated actuator and the sampling interval. The metrics

$$F_A(\delta) = \left|\sigma_{FOU} - max\left(\sqrt{FSM_x(\delta)^2 + FSM_y(\delta)^2}\right)\right|, \quad (1)$$

as well as

$$F_R(\beta,\delta) = \gamma_1 \cdot \left|\frac{\Theta}{2} - mean\left(R_{VT}(\beta)\right)\right| + \gamma_2 \cdot max\left(var\left(R_{VT}(\beta)\right)\right) + \gamma_3 \cdot max\left(Q_{VT}(\beta)\right) + \gamma_4 \cdot F_A(\beta,\delta), \quad (2)$$

are applied to satisfy the scenario requirements with a maximum of 50 iterations and a termination tolerance of 10^{-6}. F_A defines the amplitude penalty based on the positions of the FSM, whereas F_R defines the resolution by the Voronoi tessellation cell shapes, which themselves define the empty gaps in between the pattern trajectory. This approach is derived from a resonant scanning trajectory optimization[10]. It has been adapted to this use case to have a comparable metric, enabling an automated design process over all patterns.

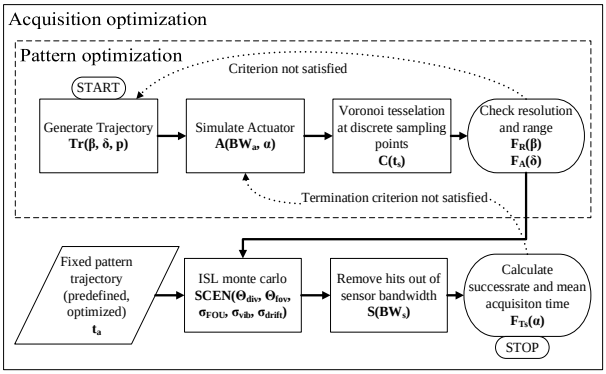

Figure 3: Program flow chart for pattern-based acquisition optimization.

In the following second part of the optimization, both patterns are considered in combination for the acquisition process. In this simulation, the pattern for T-PAT is optimized for the resolution of the divergence, whereas the pattern for T-DAT is optimized for the FOV in order to exploit the scanning resolution margin. The fixed pattern was optimized in the same way as described above, except that the actuation time $\alpha = t_a$ is fixed. A Monte Carlo program, based on previous work[11], helps to find an approximation with 1000 randomly evaluated scenario variations for this analysis. Within this simulation the ISL scan pattern is run with perturbations applied at each evaluation point. The resulting attitude error with respect to perfect alignment is given by ϕ. A successful acquisition hit is therefore determined by

$$(\phi_A \leq \Theta_{fov} \vee \phi_B \leq \Theta_{div}) \wedge (\phi_A \leq \Theta_{div} \vee \phi_b \leq \Theta_{fov}),$$

which applies design parameters from the scenario definition $SCEN(\Theta_{div}, \Theta_{fov}, \sigma_{FOU}, \sigma_{vib}, \sigma_{drift})$. Over all runs, a MAT is derived with corresponding success rate SR. The angular velocities ω_{TX} and ω_{RX} are calculated accordingly at each potential hit event. As a last processing step, recorded events outside the selected sensor S bandwidth are removed by comparing them to the maximum rates. For the evaluation of the top-level optimization

$$F_{Ts}(\alpha) = \gamma_{\alpha_1} \cdot MAT \cdot t_{lim}^{-1} + \gamma_{\alpha_2} \cdot SR^{-1} \quad (3)$$

is minimized as objective function in this work. A maximum of 20 iterations is set as limit with a termination tolerance of 10^{-4}. The MAT is divided by the maximum allowed acquisition time t_{lim} and the reciprocal of the success rate is used, so that both terms reach their minimum in the optimal configuration. The γ_α parameters can be used to fine-tune the results.

Predicted influence on acquisition hit detection

After the influence of the bandwidth on the results has been examined, the comparison of different pattern combinations will be performed. Two of the patterns make use of the resonance frequency f_R, which is a consequence of the FSM dynamics (see Table 1). Four types of patterns are distinguished: Spiral, Grid, Lissajous and Rose. Each of them combined with itself and any other pattern would result in 16 possible combinations. Preliminary investigations have shown that the Spiral search pattern can be trimmed very well for amplitude and resolution. It is therefore evaluated with each of the other patterns and with itself. The Grid pattern is the simplest and slowest of the patterns. It is the baseline because of its simple implementation. It is only considered together with the Spiral, since no significant improvements are to be expected with other combinations due to its long period duration. Finally, the combinations of the resonance driven patterns are examined. The results of all relevant evaluations are shown in Figure 4 for a maximum time t_{lim} of 600 seconds.

First of all, it can be stated that for an FOU of ±0.1 degree to ±0.2 degree all patterns show a success chance of a mutual hit of almost 100%. In particular, an FOU of ±0.1 degree gives the best results, since it is close to the range of the given FOVs. Beyond this FOU, the patterns show a decreasing tendency. If the behavior deviates from the trend, then always at the expense of its MAT. This becomes clear if one looks at the function value of the optimization over F.

The two combinations *spiral-spiral* and *spiral-rose* show robust behavior over all sensors and all FOU. For the resonant combinations, it is noticeable that the probability of success drops significantly for FOUs above ±0.2 degree. This can be explained by the fact that the relative velocities increase due to expanding FOU, while the pattern period of the fixed pattern remains constant. In the CW case, however, all combinations can show acquisitions over the whole range of FOU. Whereby the combination *lissajous-rose* and *rose-lissajous* perform best. In general, as expected, there is a correlation between sensor bandwidth and MAT, since higher bandwidths also allow smaller periods of the patterns. As shown, an upper limit of 600 seconds will result in a hit in most cases. This can then be used to align the two terminals and then switch to closed-loop tracking. At the same time, the question arises as to how a stricter requirement of 60 seconds will affect the acquisition, when the remaining time is to be reserved for the transmission of data.

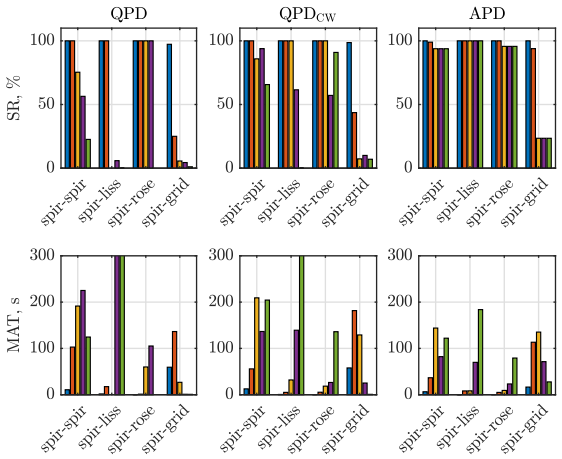

(a)

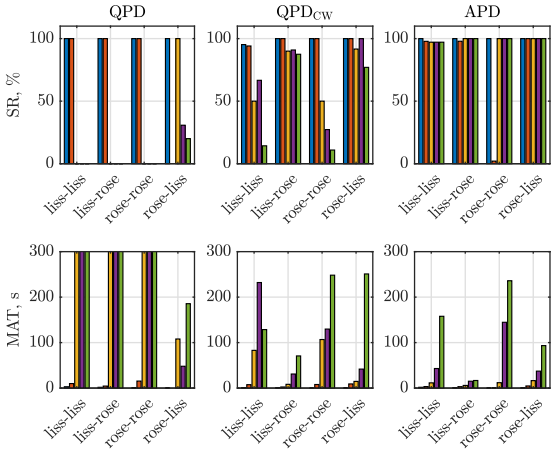

(b)

Figure 4: Performance indicators success rate and MAT for different FOU in ascending order (0.1 deg(blue), 0.2 deg(red), 0.3 deg(orange), 0.4 deg(purple), 0.5 deg(green)) and a limiting search time t_{lim} of 600 seconds. (a) Spiral combinations. (b) Resonant combinations.

Figure 5 presents the comparison of the two time limiting scenarios for the QPD_{cw} sensor. As expected, all combinations drop earlier in their success rate. From ±0.4 degree onwards, all combinations are already below 50%, whereas at 600 seconds even ±0.5 degree can be achieved with 96%. In both scenarios, the two combinations *spiral-rose* and *lissajous-rose* show the best performance. The baseline pattern is inferior in all cases.

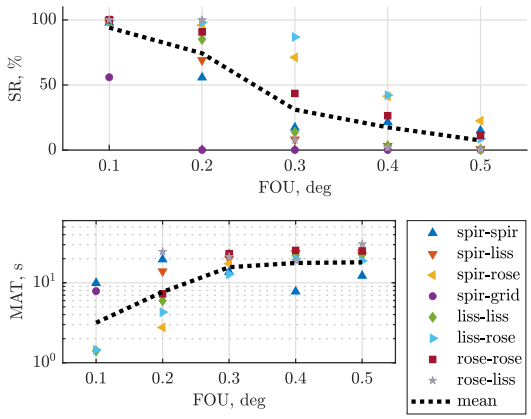

(a)

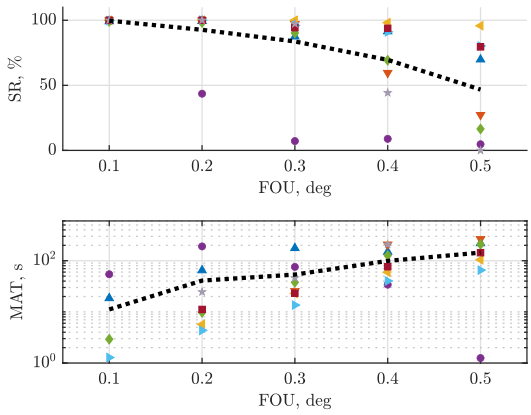

(b)

Figure 5: Comparison of the effect on acquisition due to time limitations based on the sensor QPD_{cw}. (a) t_{lim} = 60 seconds and (b) t_{lim} = 600 seconds.

Thorough analysis of the results suggests ways to improve the optimization function F. The assumed error drift of the satellite has turned out to be one of the main influencing factors. In fact, the disturbances add to the velocity of the search pattern. For a first hit this can even be helpful, as the resulting speed of the pattern is increased, and thus by chance a larger area is traversed in less time. However, this uncontrolled movement also has the disadvantage that it does not stop after a hit. Therefore, the subsequent alignment phase is correspondingly more difficult. It is desirable that a position change consists only of known or measurable changes. A proposal to reduce the influence of drift is the implementation of a secondary attitude estimation algorithm on the LCT, which can partially compensate for known drift by feed-forward FSM control and is subject to ongoing work. In addition, vibrations from the satellite platform that couple into the FSM can be reduced by active closed-loop control or passive countermeasures such as dampers.

The proposed optimization of the pattern combinations achieves a significant improvement compared to the baseline *spiral-grid*[7]. With a success probability of up to 99.9%, it demonstrates that an inter CubeSat optical ISL is feasible.

ACQUISITON MEASUREMENT CAMPAIGN

Test automation

In order to be able to operate constellations economically, an important aspect is automation of the systems involved based on a flight planner. Therefore, in the design of the campaign, one objective was that the acquisition tests could also be automated. On the one hand, this increases the confidence in the two optical terminals, and on the other hand, the number of people required to supervise the time-intensive experiments could be reduced. As several acquisition patterns were examined and each of these was repeated nine times, it resulted in runtimes of up to a full working day for a series of measurements.

For these reasons, a Python script was developed to control the actuator used for attitude manipulation, the power supply, the communication and tracking laser and the LCT itself. At the same time, all data is merged from multiple running threads and stored for later evaluation.

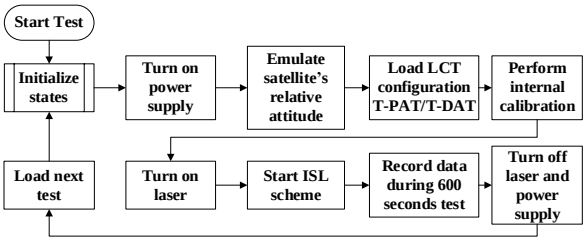

Figure 6: Automated inter-satellite link procedure for acquisition scheme validation.

The tests are loaded first. These can either contain a static offset position or a randomized trajectory within the specified FOU. Only the static variant was used for the existing test data. However, further tests with trajectories are already planned and should therefore reflect the conditions of the simulation more accurately. After the power supply has been switched on and the hexapod has moved to the corresponding start position, the configuration is loaded onto the terminal. This also specifies the type of pattern and the T-PAT or T-DAT behavior. When the laser starts, the specified maximum time of 600 seconds counts down. After the time has elapsed, which is also monitored by the Python script, the data is saved with the respective configuration

paramters and the next test is loaded. The ISL acquisition scheme is defined by Figure 7.

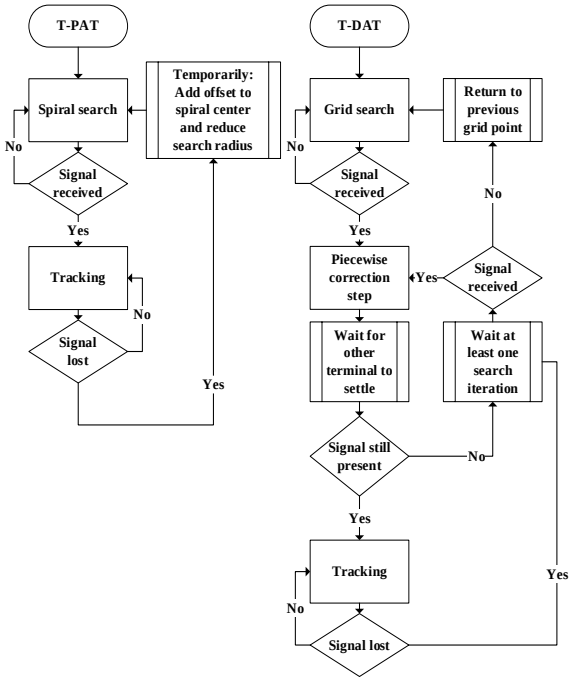

Figure 7: Implemented software acquisition scheme distinguishing between T-PAT and T-DAT, which was used during the campaign.

Experimental setup

The experiments were conducted over a distance of 334 meters in Oberpfaffenhofen between two rooftops with a direct line of sight. The FSO link architecture and setups are illustrated in Figure 8. The CubeISL T-PAT terminal utilized a motorized rotatory stage (LSDH-200WS), a motorized goniometric stage (LSDJ-15HW-02), and a motor controller (8SMC5-USB-B9-2, Standa, Lithuania) for precise alignment in azimuth and elevation angles. On the other end, a high-precision hexapod (HXP50-MECA, Newport) was employed with T-DAT to orient the terminal. The successful automation of both setups showcases high flexibility in achieving accurate pointing within tens of microradians across different assemblies. Each terminal is enclosed within a light-tight box with an OD2 filter on the aperture to ensure eye-safe operations[9]. Due to the short distance of the FSO link, the attenuation from the filters replicates the optical power that the terminals would encounter in orbit. While very short OISLs of a few meters have been successfully established within the controlled environment of a laboratory, the near-field effects of the short links distort and simplify the acquisition procedure compared to the in-orbit scenario. This can be attributed to the extended system aperture of the terminals for short-distance links, as opposed to the approximately point-size nature of the aperture over large-distance optical ISLs.

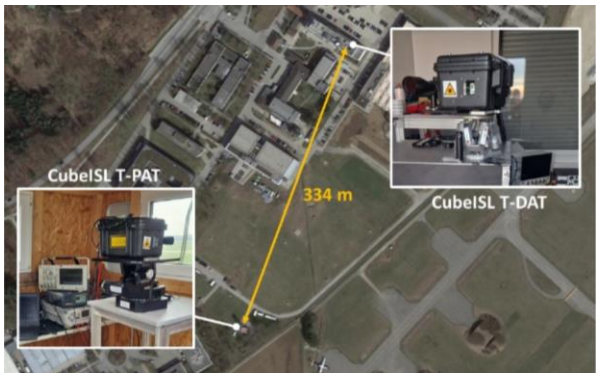

Figure 8: Architecture of the FSO link between the CubeISL terminals T-PAT and T-DAT.

For a system aperture diameter of 2 cm, a full transmitter divergence of 192 µrad, and a link distance of 4 m, the spot size at the receiver is 2.08 cm. The similar size of the spot and the receiver's aperture diameter leads to a Gaussian distribution of light over the receiver's aperture, in contrast to the expected planar wave profile typical of the far-field. Moreover, during the acquisition process, the spiral patterns are adjusted with increments that correspond to the system's divergence and FOV. For a 4 m link distance, subsequent spiral revolutions, shifted by the divergence angle, still completely overfill the receiver's aperture. Unlike the orbital scenario, some light can still be detected by the QPD detector over subsequent increments. In orbit, T-PAT would only detect T-DAT's light on a single spiral increment and would lose the signal on any subsequent increments. The medium-range distance of 334 m represents a suitable compromise that replicates far-field effects of the OISL while reducing test complexity, as the tests could be performed within the premises of the DLR campus.

Acquisition performance analysis

The results described present a preliminary state that validates the general feasibility of the acquisition scheme and the experimental setup itself. Note that the final performance analysis will be performed when the end to end acquisition campaign is carried out. Nevertheless, these experiments gave useful insights to further improve the implemented routines.

Figure 9 shows the result of an optimized pattern pair as generated by the simulation. In this case, a combination of a spiral and a rose pattern. It can be seen that the spiral pattern was optimized for T-PAT, i.e. the divergence of the beam, whereas the rose pattern is designed for T-DAT and therefore for its FOV. For the output offset, a position was selected that lies outside the divergence of T-PAT on the one hand and outside the FOV of T-DAT on the other.

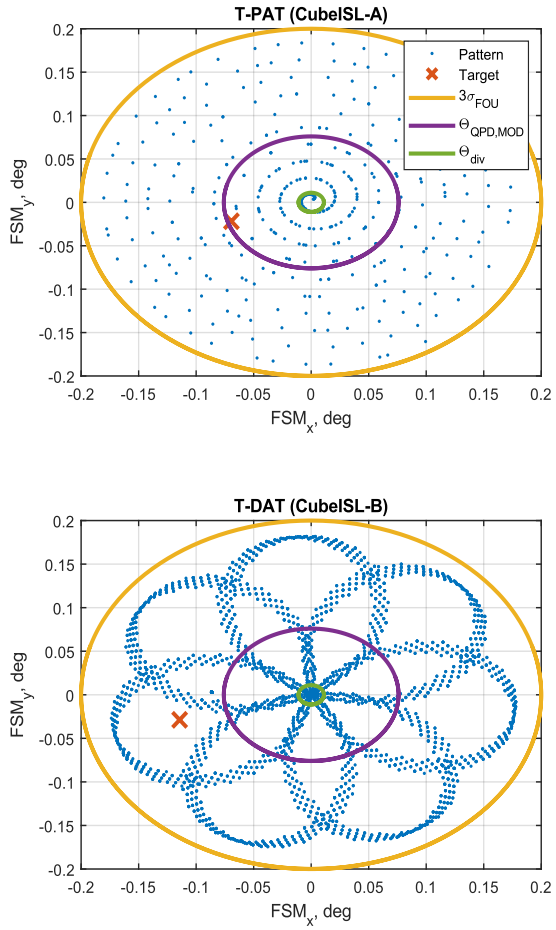

Figure 9: Optimized pattern combination of a spiral and a rose scan. Marked with a red cross are the attitude offsets for the used test configuration.

Figure 10 shows an excerpt of the behavior of the three pattern combinations considered. The sum signal of the QPD and the hits detected in it are shown, which occur when the opposite terminal's attitude error is within its divergence and at the same time the terminal's own position error is within the FOV.

It can be seen that in all cases the T-PAT terminal registers a hit first. According to the acquisition scheme, it then switches to a search mode with a limited, smaller FOU search radius as long as no constant reference signal is available. Since a single hit as a reference can still be insufficient in terms of relative offset accuracy, it usually takes multiple of those hit sequences until the deviation can be narrowed down sufficiently. A hit sequence is then detected with T-DAT so that it can also align itself with the adjustment step. A bidirectional link can now be established and maintained within five seconds in all cases.

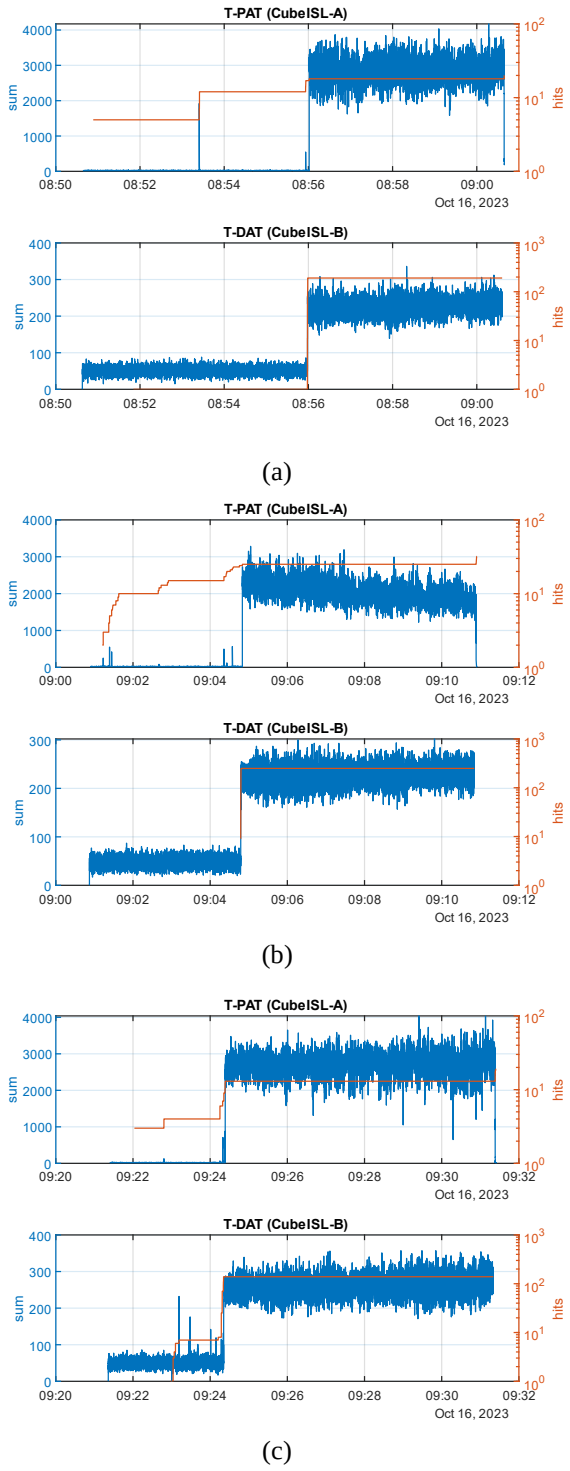

Figure 10: Acquisition measurements of (a) Spiral-Spiral, (b) Spiral-Rose and (c) Lissajous-Rose.

A statistical evaluation of this preliminary experiment in Table 2 shows a high standard deviation compared to its mean. Therefore, the results should not yet be considered final. There is a visible trend between

MAT and mean time to tracking (MTT), which appears to be increasing.

Table 2: Preliminary evaluation of nine link experiments using the described test setup.

Pattern	SR, %	MAT, s	σ_{MAT}, s	TSR, %	MTT, s	σ_{MTT}, s
SPIRAL-SPIRAL	100	11.4	16.6	100	16.8	20.5
SPIRAL-ROSE	100	12.4	10.8	100	36	19.9
LISSAJOUS-ROSE	100	14.6	22.5	100	76.5	94.1

MAT is considered as the time of a first valid attitude information as calculated by the simulation, whereas MTT marks the mean time that is needed to close the bidirectional tracking loop. The growing difference can be explained by the fact that the worse the position of the FSM is known at the time of the hit sequence, the more error-prone the position deviation determination becomes. As a consequence, multiple hit events are required for tracking. Since the MEMS FSM does not contain a feedback sensor, the control is based only on open-loop steering[12]. It is to be expected that resonant patterns deviate further from the control signal than non-resonant patterns. Thus, the difference between MAT and MTT also increases from non-resonant patterns to the combination of one and finally two involved resonant patterns. However, the tracking success rate (TSR) of 100% indicates that reliable acquisition and tracking is possible throughout all cases.

CONCLUSION

The focus of this work is on the optimization of acquisition pattern combinations for OISL acquisition and its validation in experiments. Temporally unsynchronized patterns that start at arbitrary times and initial deflections can be used and are still able to intersect with an assessable probability. Thereby, it is advantageous if the period of the two patterns deviates from each other. An algorithm is implemented to approximate an optimum of this ratio in simulation and determine optimal combinations.

In a subsequent measurement campaign over a 334 m link distance, the retrieved pattern combinations are tested within an automated experimental setup. The aim is to validate the automation process and the overall logic of the acquisition scheme, which proofed successful. 100 percent of tests were successful in the static scenario of ±0.1°. The MATs range from 11.4 seconds to 14.6 seconds, which are below the estimated baseline of 20 seconds for a *spiral-grid* pattern under optimal conditions. According to the results, it is necessary to increase the number of sample experiments to get a better estimate of the MAT. Additionally, the final MTT highly depends of the FSM deflection knowledge during a hit event. Therefore, this contribution will be taken under closer examination in the next tests. The goal is to decrease the MTT while maintaining a high TSR and a comparison with the simulation results using a random trajectory movement as disturbance.

Acknowledgments

The Authors would like to thank the entire CubeISL team at the German Aerospace Center.

References

[1] Scheinfeild, M., Kopeika, N. S. and Shlomi, A., "Acquisition time calculation and influence of vibrations for microsatellite laser communication in space," SPIE Proceedings, 195–205 (2001).

[2] Xin, L., Quanyou, S., Jing, M., Siyuan, Y. and Liying, T., "Spatial acquisition optimization based on average acquisition time for intersatellite optical communications,", 244–248 (2010).

[3] Bashir, M. S. and Alouini, M.-S., "Adaptive Acquisition Schemes for Photon-Limited Free-Space Optical Communications," IEEE Trans. Commun. 69(1), 416–428 (2021).

[4] Friederichs, L., Sterr, U. and Dallmann, D., "Vibration Influence on Hit Probability During Beaconless Spatial Acquisition," J. Lightwave Technol. 34(10), 2500–2509 (2016).

[5] Sterr, U., Gregory, M. and Heine, F., "Beaconless acquisition for ISL and SGL, summary of 3 years operation in space and on ground,", 38–43 (2011).

[6] Hechenblaikner, G., "Analysis of performance and robustness against jitter of various search methods for acquiring optical links in space," Applied optics 60(13), 3936–3946 (2021).

[7] Benjamin Rödiger, René Rüddenklau, Christopher Schmidt, Marc Lehmann, "The 4S Symposium 2022 – B. Rödiger 1 ACQUISITION CONCEPT FOR OPTICAL INTER-SATELLITE COMMUNICATION TERMINALS ON CUBESATS," Small Satellites Systems and Services - The 4S Symposium 2022 (2022).

[8] Schmidt, C., Rodiger, B., Rosano, J., Papadopoulos, C., Hahn, M.-T., Moll, F. and Fuchs, C., "DLR's Optical Communication Terminals for CubeSats,", 175–180 (2022).

[9] Nonay, J. R., Rüddenklau, R., Sinn, A., Jakobs, J. P., Berlitz, J., Rödiger, B. and Schitter, G.,

"Horizontal free-space optical link with CubeISL over 143 km," J. Opt. Commun. Netw. 16(5), 593 (2024).

[10] Tuma, T., Lygeros, J., Sebastian, A. and Pantazi, A., "Optimal scan trajectories for high-speed scanning probe microscopy,", 3791–3796 (2012).

[11] Ma, J., Lu, G., Yu, S., Tan, L., Fu, Y. and Li, F., "Acquisition performance analysis for intersatellite optical communications with vibration influence*," Chinese Phys. B 29(1), 14205 (2020).

[12] Milanovic, V., Matus, G. A. and McCormick, D. T., "Gimbal-Less Monolithic Silicon Actuators for Tip–Tilt–Piston Micromirror Applications," IEEE J. Select. Topics Quantum Electron. 10(3), 462–471 (2004).